Hindawi
Mobile Information Systems
Volume 2022, Article ID 3623963, 11 pages
https://doi.org/10.1155/2022/3623963

Research Article

Surface Plasmon Resonance Sterilization 3D Imaging Technology Considering the Engineering Hue Algorithm

Liang Xu,[1] Hongwei Wang,[2] and Wenhui Si[1]

[1]*Suzhou Polytechnic Institute of Agriculture, Suzhou, Jiangsu, China 215008*
[2]*Suzhou OPS Plasma Technology Co., Ltd., Suzhou, Jiangsu, China 215000*

Correspondence should be addressed to Wenhui Si; 11196@szai.edu.cn

Received 30 January 2022; Revised 15 March 2022; Accepted 22 March 2022; Published 20 April 2022

Academic Editor: Hye-jin Kim

Copyright © 2022 Liang Xu et al. This is an open access article distributed under the Creative Commons Attribution License, which permits unrestricted use, distribution, and reproduction in any medium, provided the original work is properly cited.

The high-resolution dynamic observation of the phenomenon of impossible surface plasmon resonance sterilization is conducted which resulted from the quality problems in the imaging process of traditional surface plasmon resonance sterilization 3D imaging technology. Surface plasmon resonance (SPR) technology is mainly based on the physical-optical properties generated by the optical coupling of metal thin films, and flexible optical analysis methods are used to improve the quality and efficiency of SPR sterilization 3D imaging. In this paper, the engineering hue algorithm is introduced into the 3D imaging process of surface plasmon resonance sterilization, and the front-end imaging system composed of the objective lens, distributed elements, focusing mirrors, and probes is used to obtain the corresponding surface plasmon resonance sterilization spectrum data on the back-end processor and quickly send the imaging calculation amount from the front-end to the back-end. Meanwhile, combined with 3D imaging, dislocation data processing technology, and multiframe reconstruction method, the reconstruction accuracy is improved, and memory space is released to speed up data processing. Finally, the experimental analysis shows that the engineering hue algorithm is used in the process of surface plasmon resonance sterilization 3D imaging, which can complete the superresolution plasmon resonance sterilization 3D imaging, and the obtained imaging effect is good, the data processing speed is fast, and it can be observed in surface plasmon resonance sterilization imaging with wide amplitude, high resolution, and low power consumption.

1. Introduction

Surface plasmon resonance (SPR) is a collective oscillation of electrons on the metal surface excited by light. Liedberg applied the SPR technology to gas detection. SPR began to get more and more attention as a spectral analysis method. In the past 30 years, SPR technology has made many achievements in the fields of pharmacy and biology and has been widely used in the real-time monitoring of biomolecular interactions. Its application fields include medical diagnosis, drug development, environmental monitoring, and food safety. The advantage of SPR technology is that the biological molecules to be detected do not need to be labeled. Label-free is of great significance for the detection of biomolecules, because markers usually have a negative impact on the original structure or activity of molecules, resulting in inaccurate measurement results. The real information of biomolecules can be obtained in real time, which is an important reason why SPR technology has continued to become a hot spot of scientific research in the past 30 years [1, 2].

The application of SPR technology in engineering mechanics, biology, chemistry, photoelectric informatics, and other fields is closely related. Its development is bound to be restricted and affected by the following aspects. SPR is an optical physical phenomenon. Biological information needs to be converted into digital signals for calculation, processing, and display through the change of light (wavelength, angle, intensity, and phase) [3, 4]. The reasonable selection of detection mode and the accurate conversion of photoelectric information are very important to SPR technology. As a high-sensitive detection technology in micro- and nanoscale, the development and improvement of SPR technology are inseparable from the auxiliary engineering

process. In particular, the application of MEMS has been proved to play a great role in promoting SPR technology. SPR technology is combined with mass spectrometry, liquid chromatography, and nanoparticle technology to give full play to their respective advantages and complement each other, improve the reliability of detection, and expand the application field. Combined with mass spectrometry, SPR technology can be used for proteome measurement and, combined with nanoparticles, is one of the important ways of SPR signal amplification [5, 6]. The notable feature of surface plasmon resonance sterilization 3D imaging is the integration of mapping and spectrum, which can effectively obtain scene radiation and spectral data information. However, with the continuous improvement of the demand for the spatial resolution and spectral resolution of surface plasmon resonance sterilization 3D imaging, when the frequency of surface plasmon resonance sterilization 3D imaging is 2 times higher than the signal frequency, the original signal can be completely recovered [6, 7]. The proposed engineering hue algorithm can quickly and accurately reconstruct the initial signal without considering the Nyquist data sampling theory, which is beneficial to signal batch compression and reconstruction. Therefore, the engineering hue algorithm and plasmon resonance sterilization 3D imaging can be combined to save the high cost and volume of hyperspectral sensors. By reducing the amount of data and information collection, the calculation amount is converted from the data collection end to the back-end processing PC. The amount of data information obtained through compression processing is less than that obtained in the previous camera system, and the pressure and power consumption of data information transmission will be reduced [8, 9]. In China, Yin Jihao proposed a method of band reconstruction using the engineering hue algorithm; Jia Yingbiao proposed a hyperspectral engineering hue algorithm reconstruction method based on previous algorithms with similar structures between spectra. Jiang Shanchao used the engineering hue algorithm in the grating spectral reconstruction process. In addition, foreign researchers have also applied the engineering hue algorithm to the postoperative plasmon resonance sterilization process of the spine. According to the principle of the engineering hue algorithm, the structural similarity feature information is optimized and reconstructed and is used in the fluorescence microscope imaging process, but a simple evaluation of spectral curves, signal-to-noise ratio, and other indicators is only used in the surface plasmon resonance sterilization 3D imaging according to the method, without the test of reconstructed hyperspectral data information, and the construction process of the model needs also to be further improved.

In this paper, a surface plasmon resonance sterilization 3D imaging technology is proposed based on the engineering hue algorithm. Based on the reconstruction of the application performance of the data cube, encoding modules, dispersing elements, and probes are used by the technology to process the spectrum data information during the imaging process for encoding. Dispersion and data sampling are performed, and 3D imaging is performed according to the data obtained by sampling. By effectively combining reconstruction technology and dislocation data preprocessing technology, the processing is achieved with low memory and computational complexity of the data, while reconstruction is achieved based on images from multiple frames of the probe. The original image is restored with high definition, and finally, a comparison experiment of hyperspectral classification and recognition test is carried out based on the original data.

2. Basic Principles and Related Algorithms

2.1. Fundamentals of Surface Plasmon Resonance. Surface plasmon resonance technology is used to realize the interaction between molecules mainly based on the physical reflection optical phenomenon caused by the total reflection of the metal film surface [10, 11]. The p-polarized light parallel to the surface is incident on the prism layer at an incident angle higher than the critical angle, the light is totally reflected, and the whole is reflected into the prism. Then, refraction is completed on one side of the prism. The electric field is completed under all reflection conditions, so that the corresponding amplitude is relative to the metal medium that does not disappear at the interface of metal and prism at the same time. The preprocessing evanescent wavelength of data transmission decays exponentially, and the evanescent wavelength interacts with electrons in the metal thin film to form an electromagnetic wave that can generate amplitude on the metal surface. According to the data analysis of the electromagnetic wavelength theory, if the electromagnetic wavelength has the same frequency and wavelength, the resonance phenomenon occurs because the surface plasmon frequency triggered by the evanescent wavelength is synchronized with the evanescent wavelength. It can also be said that based on satisfying $k_x = k_{sp}$ (k_x and k_{sp} conduct the preprocessing data transmission in the x-axis direction satisfying the preprocessing evanescent wave and surface plasmon in turn). Meanwhile, the wave vector component parallel to the surface, the evanescent wave, and the surface plasmon interact and are destroyed when all the reflection conditions are met at the interface between the prism and the thin film metal, and the phenomenon of attenuated reflection occurs. Therefore, the incident light data transmits the corresponding surface plasmon, and the reflection minimum value appears.

In general, the surface plasmon resonance curve represents the reflectivity, which changes according to the change of the incident angle, as shown in Figure 1. During the scanning process of the incident angle, the light reflectance is expressed as $R(\theta)$ principal:

$$R(\theta) = \left|r_{1,4}(\theta)\right|^2, \tag{1}$$

$$r_{1,4} = \frac{r_{i,i+1}(\theta) + r_{i+1,4}(\theta)\exp\left(2jd_{i+1}k_{zi+1}(\theta)\right)}{1 + r_{i,i+1}(\theta)r_{i+1,4}(\theta)\exp\left(2jd_{i+1}k_{zi+1}(\theta)\right)}\left(i = 1, 2\,; j = (-1)^{1/2}\right), \tag{2}$$

$$r_{i,i+1}(\theta) = \frac{\zeta_{i+1}(\theta) - \zeta_i(\theta)}{\zeta_{i+1}(\theta) + \zeta_i(\theta)}\left(i = 1, 2, 3\right), \tag{3}$$

$$k_{zi}(\theta) = \frac{2\pi}{\lambda}\sqrt{\varepsilon_i - [(\omega/c)\sqrt{\varepsilon_0}\sin(\theta)]^2}, \quad (4)$$

$$\zeta_i(\theta) = \frac{\varepsilon_i}{k_{zi}(\theta)}(i = 1, 2, 3, 4). \quad (5)$$

According to the above formula, during the data propagation of k_{zi} in the x-axis direction, the parallel wave vector components corresponding to the surface of the propagation medium i ($i = 12, 3, 4$), $r_{i,i+1}$ represents the reflectance corresponding to the $i/i+1$ surface, which is the dielectric constant $\varepsilon_i(i = 1, 2, 3, 4)$ of the i-layer propagation. $d_{i+1}(i = 1, 2)$ represents the thickness of the i-layer ($i = 1$) and the ($i = 2$)-layer, and λ is shown as the wavelength of the test light source. From the above analysis, it is found that the generation of resonance has a certain relationship with the angle of the incident light, the dielectric constant of the metal layer, and the refractive index of the medium.

2.2. Engineering Hue Algorithm. The theoretical characteristic of the engineering hue algorithm is that the data information that needs to be collected in special scenarios according to batch signals is less than the traditional sampling data information, which is the advantage of this algorithm. Using an engineered hue algorithm, surface plasmon resonance sterilization 3D imaging process, data encoding, dispersion, and sampling in hyperspectral conditions, detectors can be used to acquire low-resolution images, and low-resolution imaging is optimized for the spectral image of high spatial resolution. As shown in Figure 2, the scene of surface plasmon resonance sterilization 3D imaging is mainly based on the debug focus coding of the objective lens. The modulation of the debug template shows that the optical signal obtained after the modulated spectral signal is corrected with a collimating mirror and projected to the distributed spectrum in the distributor, and the obtained optical signal can be focused on the detector plane by a focusing mirror. The focal surface obtains a 3D compressed image signal after receiving the modulation of the spatial signal and the spectral signal, because the detector is limited in terms of pixel size. The actual compressed image signal received is usually the data information obtained after processing [12–14].

The size of the image coding processing module mainly affects the actual spatial resolution in the reconstructed spectral image, and the size of the detection unit has a constant impact on the actual data information required for 3D imaging [15]. In the traditional optical imaging algorithm, the sampling frequency of the camera probe needs to be more than twice the highest frequency of the signal, and only in this case can the optical signal be completely recovered. However, in order to obtain higher sampling frequencies, the probes used need to have a high sampling resolution. In fact, according to the limitations of the beam and process, the detector image resulted from the detection by the detector that performs the same high-resolution imaging as the encoding module usually requires data sampling. In the past, multiple imaging detections were required for data collection, but now, only a detection module is required to complete the data collection. Therefore, compared with the commonly used methods, the data information collected by the imaging detector will be greatly reduced. Because of the advantages of the engineering hue algorithm itself, the image and encoding module reconstructed by the low-resolution detector are obtained according to the sampling. For the same spectral image, it can be said that the resolution of the obtained image will not be reduced due to the reduction of the amount of data collection [16].

For the quantized hyperspectral image $f_{1\times N\cdot M\cdot L}$, it has a sparse property on $\psi_{N\cdot M\cdot L\times N\cdot M\cdot L} = \psi_1 \otimes \psi_2 \otimes \psi_3$, the I corresponding sparseness can be represented, the operator is the Kroneker product, the corresponding sparseness can be expressed as coefficients, M and N represent the image space dimension, and L represents the spectral dimension $f = \psi\theta$ $\theta_{1\times N\cdot M\cdot L}$.

In the corresponding coding, dispersion, and data sampling process, it is assumed that $T_{N\cdot M\cdot L\times N\cdot M\cdot L}$ under encoding and $S_{N\cdot(M+L-1)\times N\cdot M\cdot L}$ in the process of dispersion processing are regarded as a whole, and at the same time, its projection process is represented by $H_{N\cdot(M+L-1)\times N\cdot M\cdot L}$, then according to the data sampling process $D_{X\times N\cdot(M+L-1)}$, the engineering hue algorithm can be used to obtain low-resolution data represented by $g_{1\times X}$:

$$g = DHf = DH\psi\theta. \quad (6)$$

Among them, X represents the image dimension of data acquisition, D represents the matrix of data acquisition, H represents the projection matrix of the image, and the matrix represents the matrix product operation.

According to the engineering hue algorithm, f represents the image reconstruction represented by ψ, and the sparse representation coefficient is represented by θ, but the coefficient θ can be converted to solve the least squares problem:

$$\arg\ \min_\theta \frac{1}{2}\|g - DH\psi\theta\|_2^2 + \gamma\|\theta\|_1. \quad (7)$$

γ in the formula is expressed as a normalization coefficient. The sparse representation coefficient θ is obtained by calculation, and the reconstructed data of the image can be calculated using $f = \psi\theta$. In the surface plasmon resonance sterilization 3D imaging system, the accuracy of spectral data information mainly depends on the spectral dimension and also has a certain influence on the target recognition ability. When the optical elements and detectors meet the spectral range conditions, the engineering hue algorithm can be used to achieve the optimal value of the spectral dimension of the 3D imaging of surface plasmon resonance sterilization, and the data of the unit and the detector can be modulated according to the encoding module corresponding to the dispersion direction of the image. The greater the degree of modulation, the smaller the size of the pixel, and the higher the dimensionality obtained.

In the process of surface plasmon resonance sterilization 3D imaging, the method of 3D imaging can be used to cache the memory area and computational complexity. According to the principle of 3D imaging, the detection data analysis is

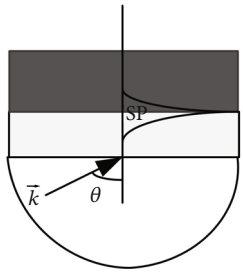

Figure 1: The principle structure of surface plasmon resonance.

modular. After processing between blocks, coded dispersion is used to collect data, and spectral information required for the detection image is obtained, but the spatial information is not substantively fused. The amount of computation and the memory are reduced. The coded dispersion is used to collect data and obtain the spectral information required for the detection image, but the spatial information is not substantially fused. The consequence of 3D imaging is to reduce the dimension of data matrix transformation, thereby reducing the amount of computation and memory. In addition, since the multiframe detector images are used for image reconstruction at the same position many times, the coded data information corresponding to the images of each frame is different, and the corresponding imaging results are also different. Therefore, the scene accuracy obtained by using multiframe images is also more than that of single-frame images. Compared with the whole image imaging process, in block imaging, the projection matrix corresponding to the 3D imaging is small in size, but it is beneficial to the operation of data storage with the hardware device. In 3D imaging, the data reconstruction of the whole image is not required, but after the block test is completed, it can be transmitted to the corresponding data processing process, so as to realize the dynamic observation of the spectral data (Figure 3) [17, 18].

In this case, if any block is misplaced, it will cause the scene image f^j and the sampled data block $g^i, i = 1, \cdots, t$ in the same position. The corresponding expression is

$$g^i = dH^i f^j = dH^i \psi\theta. \tag{8}$$

The number of photographing frames is represented according to expression (8). The scene-encoding template block corresponding to the compressed image represents the ith frame, and d represents the data collection block matrix, $i = 1, \cdots, t$, H^i, f^j. The 3D imaging transformation is expressed as

$$\arg\ \min_\theta \frac{1}{2} \left\| g^i - dH^i \psi\theta \right\|_2^2 + \gamma \|\theta\|_1, \tag{9}$$

$$f^j = \psi\theta, i = 1, \cdots, t. \tag{10}$$

The implementation steps of the corresponding engineering hue algorithm are

(1) Initialization stage: set the basic variable parameters, read the initialized data, and complete the setting of the encoding matrix

(2) Imaging process:
   (a) Coded dispersion processing
   (b) Obtain the data acquisition image g

(3) Reconstruction procedure:
   (a) Dimensionally spaced row cycle for sample data collection
   (b) Dimensionally spaced column cycle for sample data collection
   (c) Construct the data acquisition block matrix d
   (d) While constructing the spectral order and matrix, combine the corresponding coding matrix blocks to construct the projection matrix under continuous multiframe reconstruction. Here, it is necessary to connect each row after quantizing the projection matrix corresponding to the image of each frame. $H^i, i = 1, \cdots, tH^i$
   (e) Constructing a 3D sparse orthogonal basis ψ
   (f) Utilizing the 3D imaging block f^j of the projected gradient method
   (g) Imaging in 3D

2.3. 3D Imaging of Surface Plasmon Resonance Sterilization. In the case of electropolymerization and self-assembled films corresponding to conductive polymerization, the engineering hue algorithm can also quantitatively reflect the precipitation of the copolymer and the electrochromic properties of the polymer, as shown in Figure 4(a), and the continuous increase of the reflectivity of the different group can realize the deposition of substances on the surface of the substrate during the process of potential scanning. In the process of continuous circulation, it can be seen from the surface plasmon resonance sterilization 3D imaging curve that the thickness of the modified layer also increases with the increase of P3T grouping. The number of P3T groups has a great influence on the thickness of the electrodeposited layer, and the doping and deoxidation processes bring changes to the polymer, which can be detected by using the reflectivity change of the polymer. The significant change of P3T makes the electrochromism effect, which can be adjusted with reference to the potential of 0 V→2.8 V, and the corresponding colors will appear white, red-orange, and blue-green in turn. The plasma is white at 0 V and 8 V and will turn green at 1 V. At the initial potential of doping and dedoping, it can be seen that the reflectivity of P3T will change greatly. It can be seen that when the P3T layer is used, the dielectric constant will change greatly in the stages of doping and dedoping. However, the change in the reflectivity of the plasma during this process is very small, and the

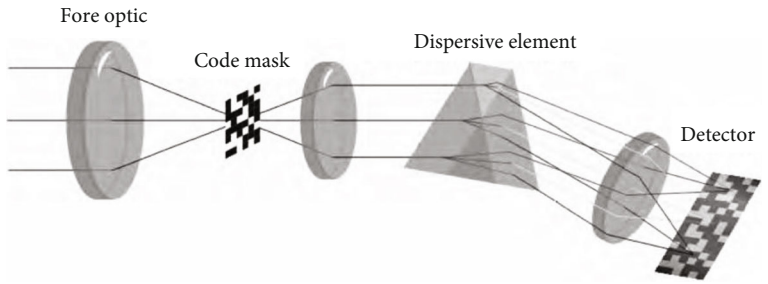

Figure 2: Principle of engineering hue 3D imaging system.

main reason is related to the number of charges. During the plasma doping and dedoping stages, the amount of charge transfer is small, and the corresponding change in the reflectivity of the copolymer is between P3T and the plasma. Therefore, the P3T copolymer plays an important role as the dielectric constant changes. The contra-doping rate shows that the change in the dielectric constant of the polymer layer is mainly closely related to electrochromism. As can be seen from Figure 4(b), after washing the electropolymerized polymer layer with vinylidene chloride, the treatment of increasing the constant potential in the acetonitrile solution excluding the monomer (TBP) is shown in Figure 4(b), and the deducing SPR angle change curve corresponds to this stage of sedimentary deposit.

The sterilization 3D imaging process under the treatment of cyclic voltammetry and engineering hue algorithm is mainly based on electrochemical polymerization under the functionalization of carbazole in the multilayer film. The cross-linking process in the multilayer film is shown due to the increase of the current during this cycle period. From the comparison of electropolymerization treatments, it was found that the dielectric constant and thickness of the multilayer films varied to different degrees under the influence of the oligomeric diene layer. Generally speaking, the reflectivity of the multilayer film will decrease during the oxidation-doping process; however, the reflectivity between reduction and dedoping increases, and the corresponding reflectivity change has a certain relationship with the film thickness.

SRP technology is sensitive to the change in refractive index around the surface plasmon, and the engineering hue algorithm is applied to the electrode surface for adsorption and desorption stages. If the polymer is added to the surface plasmon, the intensity of the SRP signal will become stronger. The main reason is that the polymer is adsorbed on the electrode surface, and there is a continuous polymer solution. At this time, the SRP signal will not change. However, if the positive and negative potentials are added to the electrodes, the signal of the SRP will be changed.

The engineering hue algorithm can be used to accurately monitor the change in the thin adsorbate on the metal surface. For example, the thickness of the cytochrome due to redox only changes by 0.06 mm, the electropolymerization change in the alignment direction of the thickness of the self-assembled layer caused by redox in the detection layer can be obtained, and the obtained maximum water content in the SAM is injected into the space [19]. The expression can be used as

$$\Delta\theta = c_1\Delta n + c_2\Delta d, \tag{11}$$

$$\Delta n = -\frac{1}{6n}\left(n^2+2\right)^2\left(\frac{n^2-1}{n^2+2} - \frac{n_w^2 - 1V_f}{n_w^2+2V}\right)\frac{\Delta d}{d}. \tag{12}$$

According to the above expression, when the angle of SRP changes, the refractive index and layer thickness are changed due to SAM rearrangement or reconstruction, with c1 and c2 as constants, and are consistent with the volume V of the modified layer, and d represents the layer thickness of the SAM before redox. According to Figure 4, it can be seen that there is a certain relationship between the change of the obtained SRP angle and the change in the layer thickness. According to Figure 4(b), it can be seen that the change of the SRP angle in the figure is huge, and the redox will immediately lead to the change of the monolayer coincidence and film thickness. In the solution of 0.12 mol L-1 HCIO 5 and 0.12 mol L-1 HNO4, 0.091 nm and 0.081 nm can be evaluated sequentially with the change of layer thickness. So, during the electrochemical oxidation of the SAM layer, even though the alkyl chain changes in the direction away from the electrode, or the dimethyl mercaptan moves or rotates around the fusion of the dimethyl mercaptan group and the alkyl chain; it can be seen that the led essence before and after the change is the process of change of film thickness [20, 21].

As a flexible technology for monitoring the corresponding analytes adsorbed on the plasma surface, plasmon resonance sterilization 3D imaging technology can detect plasma together with an anodic solution using voltammetry, and high-resolution differential SRP technology is effectively used for the detection of the metal plasma contained in the water; the plasma adjusts the potential around the SRP sensing chip by using the method of electroprecipitation, and the change of the angle of the SRP and the electroprecipitation type and quantity of plasma contained are determined by the quantitative detection method for the change of the SRP angle and electrochemical current signal. In order to better improve the accuracy of the detection technology, it can be seen from Figure 5 that the plasma surface can be divided into a parameter area and an induction area by using other types of differential methods, and the change of the SRP angle in this area can be collected as differential signal data, to detect the optimal potential and plasma deposited

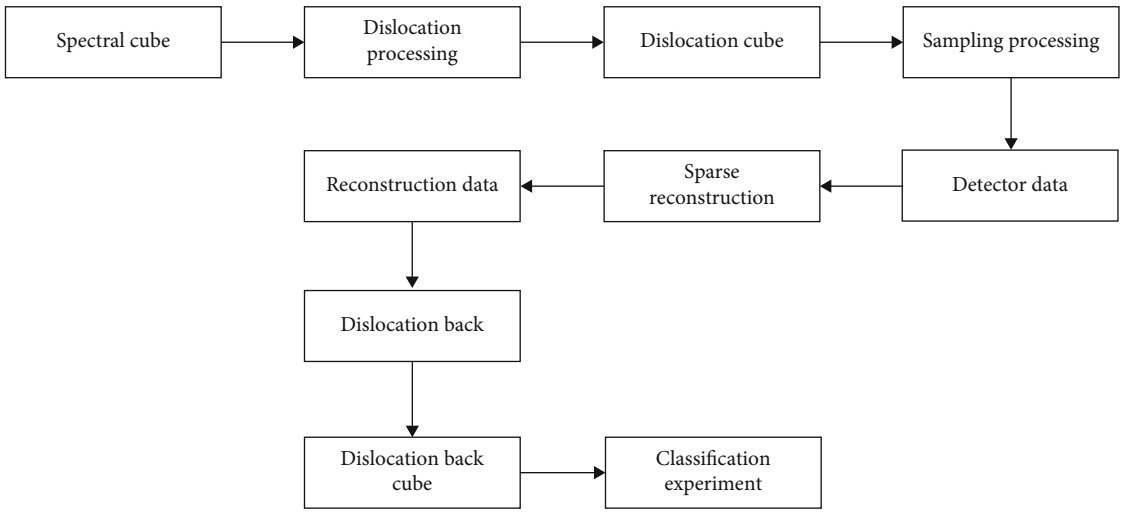

Figure 3: Flow chart of 3D imaging of plasma resonance sterilization under engineering hue algorithm.

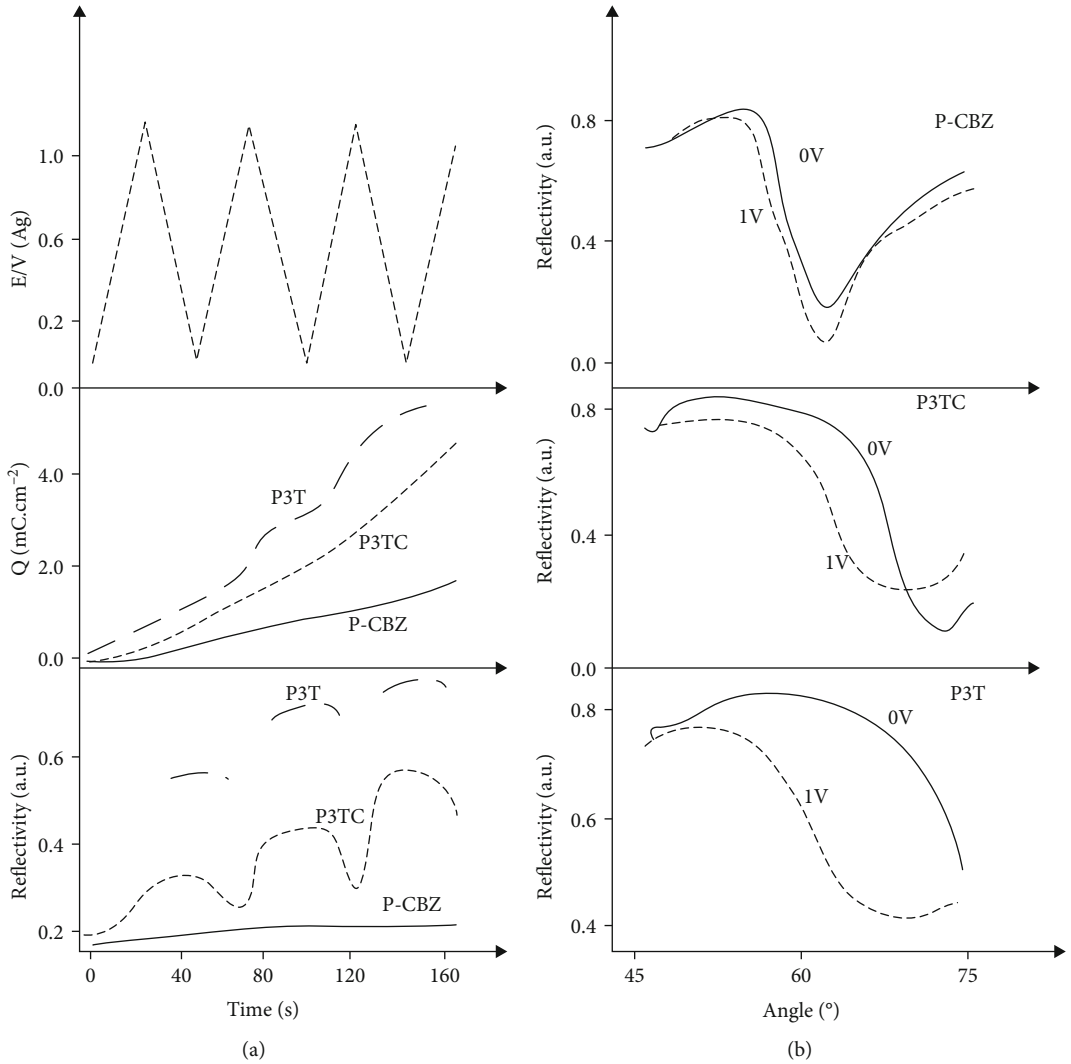

Figure 4: The test results of the combined use of the engineering hue algorithm. (a) Potential and SPR kinetic curves of electrodeposited P3T/P3TC-50/plasma in 0.1 mol L-1TBP; (b) angle curve of the electrodeposited polymer in 0.1 mol L-1TBP, monomer free acetonitrile solution.

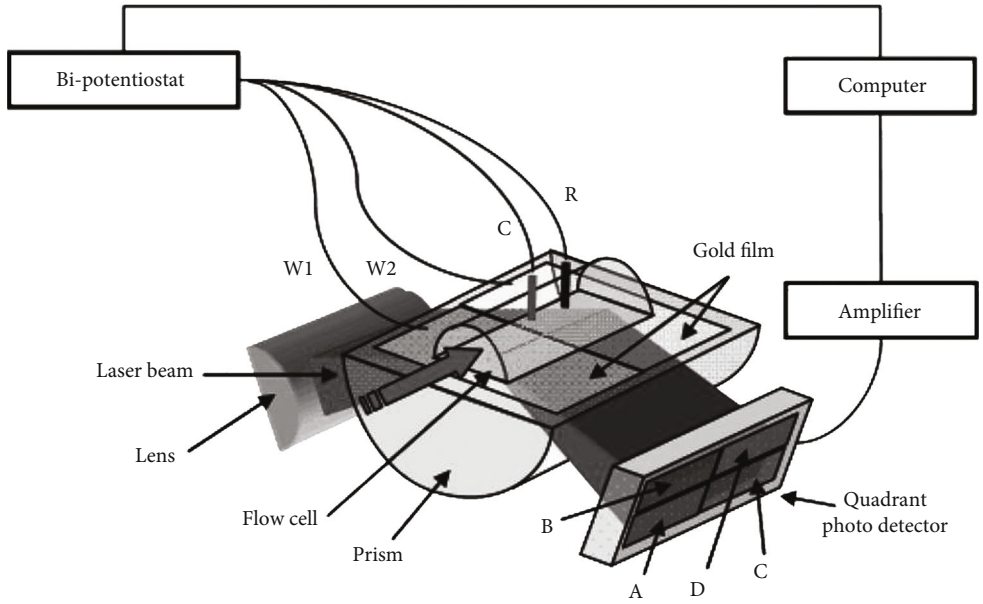

Figure 5: Schematic diagram of the differential SPR plasma surface. The four-strand photovoltaic cells.

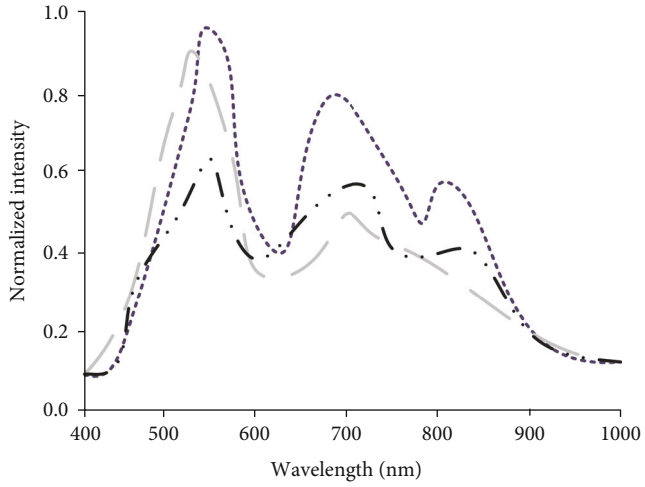

Figure 6: Resonance spectra of different incident angles.

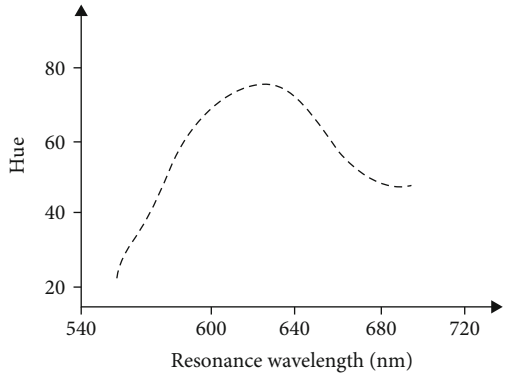

Figure 7: Resonance wavelength change in engineering hue algorithm.

on its surface. The Lorentz force is used to generate fluid motion, and magnetic fluid is used to achieve changes in convection, making the external magnetic field and electrolytic cell interact to achieve optimal resonance effect.

3. Analysis of Experiment and Results

It can be seen from Figure 6 that the resonance wavelength changes due to the change of the resonance spectrum detected at different incident angles, because the incident angle starts to become smaller. Due to the change of the resonant wavelength, the color of the image also changes, along with the corresponding image color and resonant wavelength. The engineering hue algorithm can be used to figure out the SRP 3D imaging effect. The change in the color of the image in the 3D imaging process will lead to a change in the hue distribution per unit project. The engineering hue is under the characteristics of all the pixels in the 300 pixel × 300 pixel area. As can be seen from Figure 7, due to the change of the resonance wavelength, the engineering color of the 3D imaging will change, and the obtained color will change from dark to light. However, due to the change of the engineering hue between different wavelengths, the engineering hue will also change greatly, resulting in a change in the acquired sensitivity of the engineering hue.

In the initial stage (Figure 8(a)), the resonance wavelength is 568.47 nm, and the sodium chloride concentration corresponding to the resonance spectrum of the sodium chloride solution will also increase. It can be seen from Figure 8(b) that due to the change of the resonance wavelength, the linear relationship of the refractive index can be changed. At this time, $y = y = -152.225 + 134.546x$ can be set, and the fitting expression corresponds to the similarity $R^2 = 0.998$. In this case, the resonant spectral sensitivity will become 1135 mm/RIU. From the experimental results, it can be seen that if the resonant wavelength becomes smaller in

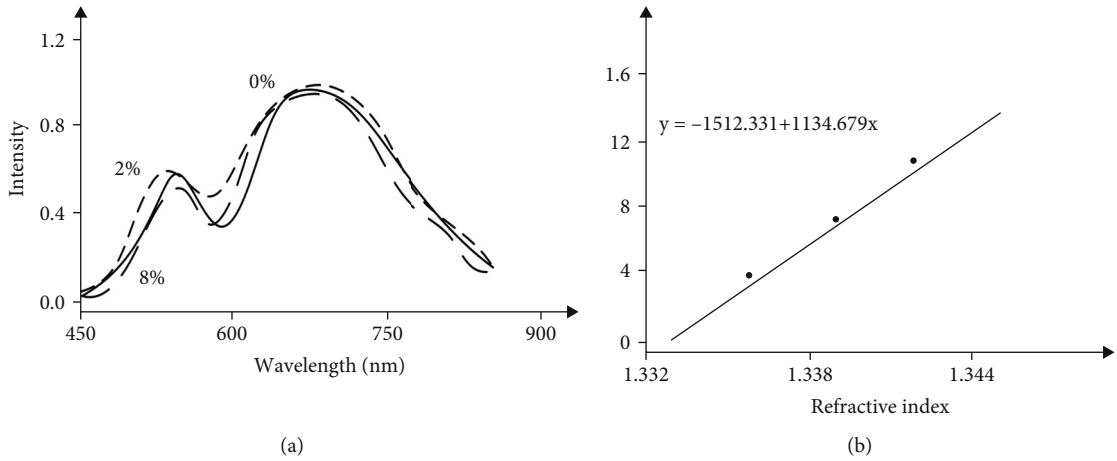

Figure 8: (a) Resonance spectra corresponding to different concentrations of sodium chloride solution. (b) The relationship between the change of the resonance wavelength and the refractive index.

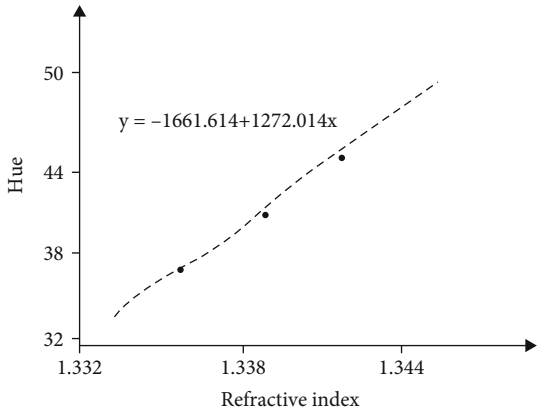

Figure 9: Relationship between average engineering hue and refractive index.

the initial stage, the resonant spectral sensitivity will become smaller, which will affect the detection accuracy of the external refractive index.

In the initial stage, the resonant wavelength is 56788 nm. At this time, the sodium chloride concentration corresponding to the resonant spectrum of the sodium chloride solution will also increase, and the engineering hue of the 3D imaging will continue to increase. It can be seen from Figure 9 that there is a linear correlation between the engineering hue and the corresponding refractive index, which changes with the change of the refractive index. At this time, $y = -161.524 + 1272.546x$ can be set, with the similarity $R^2 = 0.998$, and the sensitivity of the engineering hue is about 1272/RIU. It can be seen from the experimental results that the sensitivity of the engineering hue is a constant value compared with the sensitivity of the resonance spectrum, but it will have a serious impact on the detection of the change of the refractive index from the outside.

According to the above detailed analysis, when determining the resonance length under initialization, the relationship between the sensitivity of the resonance spectrum and the resonance wavelength of the engineering hue needs to be fully considered. Based on the sensitivity of the SRP refractive index corresponding to the engineering hue parameters, the resonance wavelength greater than 650 mm can be used for the analysis and discussion to obtain larger engineering hue sensitivity. According to the above experimental test results, when the resonant wavelength becomes longer, the corresponding engineering hue will become smaller. Therefore, 680 mm can be set as the resonant wavelength in the initialization stage to obtain the maximum engineering hue sensitivity.

According to Figure 10(a), the resonant wavelength in the initialization phase is 650.48 nm. Comparing the resonant spectrum of sodium chloride solution at different concentration values, the resonant wavelength will also change due to the change in sodium chloride concentration. According to Figure 10(b), it can be seen that the relationship between the error amount of the resonance wavelength and the refractive index can be expressed as $y = y = 2987.89 + 22241345x$, the fitting degree as $R^2 = 0.998$, and the sensitivity of about 2241 nm/RIU in a linear relationship. Compared with the sensitivity at the resonance wavelength of 567.46 nm in the initialization phase above, it was found that the sensitivity of the resonance spectrum was significantly improved.

The SPR images (300 pixels× 300 pixels) correspond to different concentrations of sodium chloride solutions at the initial resonance wavelength of 650.47 nm and their 3D engineering hue distributions. The color of the SPR image gradually changed from green to yellow as the concentration of the NaCl solution increased. The hue of engineering gradually dropped. The obtained image is also used to reflect the advantages of the SPR image. The 300 pixel × 300 pixel image is further subdivided into 100 pixels × 100 pixels, and the engineering hue sensitivity is obtained by averaging the engineering hue of all pixels in the image.

As shown in Figure 11, the relationship between the average engineering hue and the refractive index of images

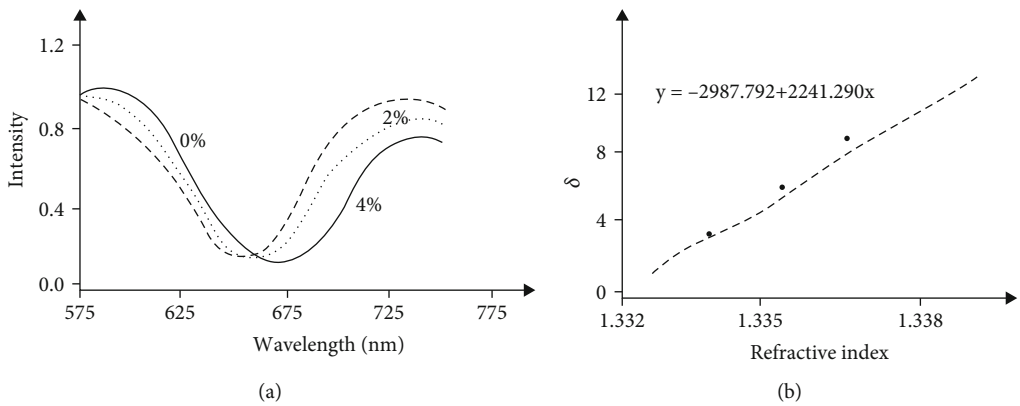

Figure 10: (a) The resonance spectra corresponding to different concentrations of sodium chloride solution. (b) The relationship between the amount of resonance wavelength change and the refractive index.

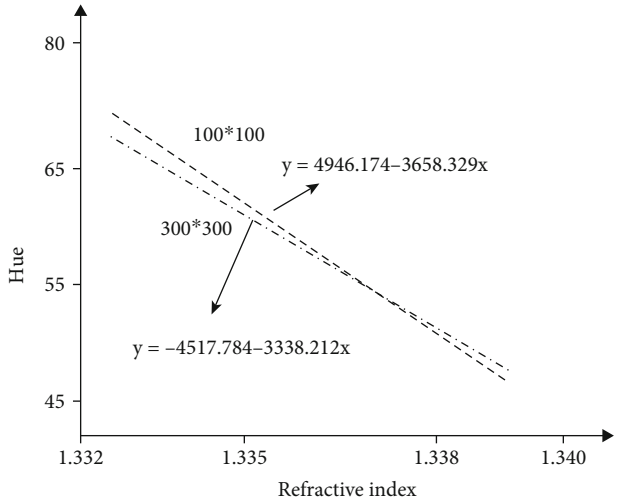

Figure 11: Relationship between average engineering hue and refractive index for images of different sizes.

of different sizes is 300 pixels × 300 pixels. The fitting equation of the relationship between the average engineering hue and the refractive index is as follows: $y = 4517.784 - 3338.212x$, the fitting degree is $R^2 = 0.997$, and according to the fitting equation, the engineering hue sensitivity is about 3338/RIU. From the comparison of resonance spectral sensitivity and SPR image engineering hue sensitivity, it is found that the latter is about 149 times that of the former. The fitting equation of the relationship between the average engineering hue and refractive index of 100 × 100 pixels is $y = 49.14 - 3658.329x$, with the fitting degree of $R^2 = 0.992$. Through the fitting equation, the engineering hue sensitivity is about 3658/RIU. At this time, the engineering hue sensitivity is about 163 times that of the resonance spectral sensitivity and shows a relatively significant improvement compared to 300 pixels × 300pixels.

As described above, at the initial resonant wavelength of 650 nm, higher sensitivity was obtained by comparing the resonant spectral sensitivity with the SPR image engineering hue sensitivity, using the image-averaged engineering hue to detect the external refractive index. Higher engineering hue sensitivity can be achieved by filtering an area in the image.

Figure 12(a) shows the SPR image of the SPR chip coated with PTFE film and its 3D engineered hue distribution. As can be seen from the SPR image, the colors in the image are distributed between the engineering hues of green and yellow due to the uneven thickness of the Teflon film. By calculating the hue distribution of the 3D engineering, it is found that the image is a green area as shown in Figure 12(a) as shown in the middle field 1, and its average engineering color is about 70.7. The areas where the image is yellow are shown in Figure 12(a) as the middle area 2, and the average engineering hue is relatively low, about 52.4. By combining the results of the above refractive index sensitivity experiments, the areas with larger engineering colors in the image include the following: the refractive index here is low, and the refractive index of Teflon is larger than that of air, thus indicating that the film thickness in this area is small. Conversely, an area of the image with a small engineering hue indicates a large thickness of the Teflon film in that area.

To further study the sensitivity characteristics of different thickness regions of the film to the refractive index, Figure 12(b) calculates the SPR image where the external environment is deionized water and the engineering hue and compares it with the same field. The engineering hue of region 1 changes from 70.7 to 48.4, and the engineered hue for Zone 2 has changed from 52.4 to 44.9. Therefore, the sensitivity of the refractive index of region 1 is greater than that of the region 2 because the film thickness of region 1 is small.

By calculating the 3D-engineered hue distribution of the SPR image, the thickness inhomogeneity of the PTFE film can be characterized, and the external refractive index can be further varied to measure the sensitivity of different thicknesses to localized regions of the refractive index. Experimental results show that regions with small film thickness are more sensitive to the relative refractive indices of their engineered hues.

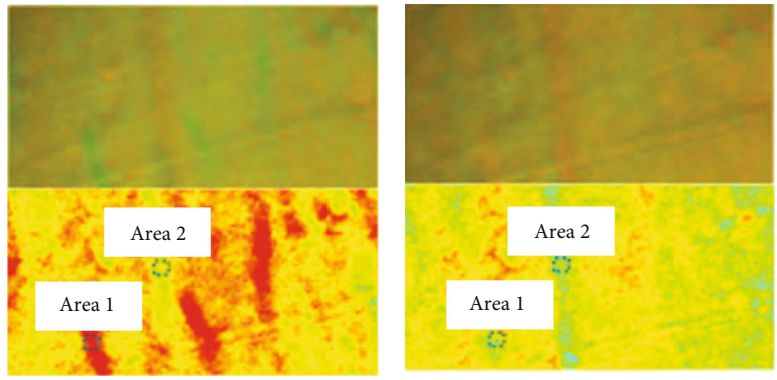

(a) (b)

Figure 12: (a) SPR image and its 3D engineering hue distribution corresponding to the case where the external environment is air. (b) SPR image and its 3D engineering hue distribution corresponding to the case where the external environment is water.

4. Conclusion

In this paper, we apply an engineered hue algorithm to the surface plasmon resonance sterilization 3D imaging process to enable the observation of physicochemical changes occurring on the surface of color SPR images. According to the engineering hue algorithm used, the sterilization imaging effect of surface plasmon resonance can be quantitatively analyzed. By adjusting the incident angle, the resonance spectrum and the resonance wavelength corresponding to the SPR image can be confirmed. According to the existing relationship, the initial resonance wavelength was selected, the sensitivity of the engineering hue was optimized, and the sensitivity of the engineering hue in the surface plasmon resonance sterilization imaging area was screened out. Finally, the experimental test results show that for 3D imaging of the corresponding SPR chip on the coated PTFE film, the calculation result of the engineering hue distribution can be directly observed, and the film thickness can be calculated. According to the data information of the calculated surface plasmon resonance sterilization 3D imaging area, the adjustment of the refractive index sensitivity under different film thicknesses was analyzed. When the surrounding environment is converted from air to water, the engineering hue of the imaging area with a smaller film thickness will decrease, and that of the imaging area with a larger film thickness will increase. It can be seen that the 100-pixel imaging with smaller film thickness is more sensitive to the refractive index, which also illustrates the feasibility of the surface plasmon resonance sterilization 3D imaging technology based on the engineering hue algorithm.

Data Availability

The data used to support the findings of this study are available from the corresponding author upon request.

Conflicts of Interest

The authors declare no conflicts of interest.

Acknowledgments

This research study is sponsored by these projects: project one: the Jiangsu Fresh Agricultural Products Preservation Engineering Technology Research and Development Center, and the project number is [2018] 10 to Su Jiaoke; project two: the Science and Technology Industry Cultivation Project of Suzhou Agricultural Vocational and Technical College, and the project number is KYPY201701; and project three: the Research and Innovation Team of Suzhou Agricultural Vocational and Technical College (Class A). We thank these projects for supporting this article.

References

[1] P. Pattnaik, "Influence of adhesion layer on performance of surface plasmon resonance sensor," *IET Optoelectronics*, vol. 12, no. 4, pp. 168–175, 2018.

[2] V. Amendola, R. Pilot, M. Frasconi, O. M. Maragò, and M. A. Iatì, "Surface plasmon resonance in gold nanoparticles: a review," *Journal of Physics: Condensed Matter*, vol. 29, no. 20, pp. 203002–203197, 2017.

[3] X. Y. Wang, Y. L. Wang, S. Wang et al., "Lasing enhanced surface plasmon resonance sensing," *Nano*, vol. 7, no. 9, pp. 12282–12296, 2017.

[4] R. Dehmel, J. J. Baumberg, U. Steiner, and B. D. Wilts, "Spectrally resolved surface plasmon resonance dispersion using half-ball optics," *Applied Physics Letters*, vol. 111, no. 20, pp. 201102-201103, 2017.

[5] L. Kaiqun, L. Yonghua, C. Junxue, Z. Rongsheng, W. Pei, and M. Hai, "Surface plasmon resonance hydrogen sensor based on metallic grating with high sensitivity," *Optics Express*, vol. 11, no. 3, pp. 620–627, 2019.

[6] T. Guo, "Fiber grating-assisted surface plasmon resonance for biochemical and electrochemical sensing," *Journal of Lightwave Technology*, vol. 35, no. 16, pp. 3323–3333, 2017.

[7] L. Chao, Y. Lin, X. Lu et al., "Mid-infrared surface plasmon resonance sensor based on photonic crystal fibers," *Optics Express*, vol. 119, no. 7, pp. 57–57, 2017.

[8] L. Ji, X. Sun, G. He et al., "Surface plasmon resonance refractive index sensor based on ultraviolet bleached polymer waveguide," *Sensors & Actuators B Chemical*, vol. 244, no. 6, pp. 373–379, 2017.

[9] S. S. Hinman, K. S. Mckeating, and Q. Cheng, "Surface plasmon resonance: material and interface design for universal accessibility," *Analytical Chemistry, Acs.Analchem*, vol. 14, no. 16, pp. 136–154, 2017.

[10] M. Kitta, K. Murai, K. Yoshii, and H. Sano, "Electrochemical surface plasmon resonance spectroscopy for investigation of the initial process of lithium metal deposition," *Journal of the American Chemical Society*, vol. 143, no. 29, pp. 11160–11170, 2021.

[11] S. Marhaba, G. Bachelier, C. Bonnet, M. Broyer, and M. Pellarin, "Surface plasmon resonance of single gold nanodimers near the conductive contact limit," *The Journal of Physical Chemistry C*, vol. 113, no. 11, pp. 317–324, 2017.

[12] S. Chakma, M. A. Khalek, B. K. Paul, K. Ahmed, M. R. Hasan, and A. N. Bahar, "Gold-coated photonic crystal fiber biosensor based on surface plasmon resonance: design and analysis," *Sensing and Bio-Sensing Research*, vol. 18, no. 3, pp. 7–12, 2018.

[13] M. Misbahuddin, A. A. P. Ratna, and R. F. Sari, "Dynamic multi-hop routing protocol based on fuzzy-firefly algorithm for data similarity aware node clustering in WSNs," *International Journal of Computers Communications & Control*, vol. 13, no. 1, pp. 99–116, 2018.

[14] L. Chao, F. Wang, P. K. Chu, L. Qiang, S. Tao, and W. Su, "Symmetrical dual d-shape photonic crystal fibers for surface plasmon resonance sensing," *Optics Express*, vol. 26, no. 7, pp. 127–130, 2018.

[15] Y. Jia, Y. Peng, J. Bai et al., "Magnetic nanoparticle enhanced surface plasmon resonance sensor for estradiol analysis," *Sensors and Actuators B Chemical*, vol. 254, no. 4, pp. 629–635, 2017.

[16] Y. F. Liu and Q. S. Zhang, "Multi-objective production planning model for equipment manufacturing enterprises with multiple uncertainties in demand," *Advances in Production Engineering & Management*, vol. 13, no. 4, pp. 429–441, 2018.

[17] L. Chao, Y. Lin, X. Lu, L. Qiang, and P. K. Chu, "Mid-infrared surface plasmon resonance sensor based on photonic crystal fibers," *Optics Express*, vol. 25, no. 13, pp. 14227–14237, 2017.

[18] G. An, S. Li, X. Yan et al., "Extra-broad photonic crystal fiber refractive index sensor based on surface plasmon resonance," *Plasmonics*, vol. 12, no. 2, pp. 465–471, 2017.

[19] T. Wu, S. Yu, W. Ying, S. Cao, and Y. Wang, "Surface plasmon resonance biosensor based on gold-coated side-polished hexagonal structure photonic crystal fiber," *Optics Express*, vol. 25, no. 17, pp. 914–923, 2017.

[20] X. Liu, F. Luo, P. Li, Y. She, and W. Gao, "Investigation of the interaction for three citrus flavonoids and α-amylase by surface plasmon resonance," *Food Research International*, vol. 20, no. 13, pp. 1–14, 2017.

[21] D. Michel, F. Xiao, and K. Alameh, "A compact, flexible fiber-optic surface plasmon resonance sensor with changeable sensor chips," *Sensors and Actuators B Chemical*, vol. 246, no. 8, pp. 258–261, 2017.